Evolution of Conduit Geometry and Eruptive Parameters during Effusive Events

A. Aravena[1], R. Cioni[1], M. de' Michieli Vitturi[2], M. Pistolesi[3], M. Ripepe[1] and A. Neri[2]

[1] Dipartimento di Scienze della Terra, Università di Firenze, Firenze, Italy.

[2] Istituto Nazionale di Geofisica e Vulcanologia, Sezione di Pisa, Pisa, Italy.

[3] Dipartimento di Scienze della Terra, Università di Pisa, Pisa, Italy.

Corresponding author: Alvaro Aravena (alvaro.aravenaponce@unifi.it)

Key Points:

- Temporal evolution of conduit geometry modeled by the effects of fluid shear stress and elastic deformation.
- Numerical modelling of conduit dynamics coupled with appropriate criteria for addressing the temporal variations of the feeding system.
- Controlling factors of effusion rate curves during basaltic effusive eruptions.

This article has been accepted for publication and undergone full peer review but has not been through the copyediting, typesetting, pagination and proofreading process which may lead to differences between this version and the Version of Record. Please cite this article as doi: 10.1029/2018GL077806

The dynamics of effusive events is controlled by the interplay between conduit geometry and source conditions. Dyke-like geometries have been traditionally assumed for describing conduits during effusive eruptions, but their depth-dependent and temporal modifications are largely unknown. We present a novel model which describes the evolution of conduit geometry during effusive eruptions by using a quasi-steady state approach based on a 1D conduit model and appropriate criteria for describing fluid shear stress and elastic deformation. This approach provides time-dependent trends for effusion rate, conduit geometry, exit velocity and gas flow. Fluid shear stress leads to upward widening conduits, whereas elastic deformation becomes relevant only during final phases of effusive eruptions. Simulations can reproduce different trends of effusion rate, showing the effect of magma source conditions and country rock properties on the eruptive dynamics. This model can be potentially applied for data inversion in order to study specific case studies.

1 Introduction

Evolution of effusive eruptions is mainly controlled by time-dependent variations of effusion rate, the dynamics of which are influenced by several processes related to magma source conditions and conduit geometry (Calvari et al., 2003; Harris et al., 2007; Harris et al., 2011; Wadge, 1981). Temporal variations of composition and thermodynamic conditions of magma in the reservoir are often related to emptying and refilling cycles (Andronico et al., 2005; Coppola et al., 2017a; Dzurisin et al., 1984; Landi et al., 2006; Ripepe et al., 2017). Conduit geometry is strongly controlled by the coupled effect of erosion processes and elastic deformation, which are functions of the country rock and magma properties (Dragoni and Santini, 2007; Piombo et al., 2016). If we assume a negligible effect of thermal erosion, for studying conduit enlargement during effusive eruptions, two main mechanisms should be considered: conduit collapse and fluid shear stress. Although some formulations have been proposed for describing the controlling factors of such erosive mechanisms, it is difficult to quantify their relative importance (Aravena et al., 2017; Macedonio et al., 1994). Conduit collapse can only occur in the presence of a large pressure difference between country rocks and magma in the conduit, and it is not expected to occur during effusive eruptions (Aravena et al., 2018; Macedonio et al., 1994). Accordingly, basaltic effusive eruptions present favorable conditions for addressing fluid shear stress, which is controlled by magma viscosity, velocity and country rock mechanical properties. Furthermore, decompression-driven elastic deformation of host rocks is expected to produce a significant effect on conduit geometry (Costa et al., 2007a), acting in opposition to fluid shear stress. Piombo et al. (2016) presented an analytical model describing conduit erosion during effusive eruptions. This model can reproduce effusion rate trends similar to those proposed by Wadge (1981) (i.e., initial increase of effusion rate and a later decreasing phase), assuming cylindrical conduits with elliptical cross section, constant values for magma viscosity and density, and time-dependent erosional processes as overpressure decreases. Although it does not consider the effect of elastic deformation, this model has been demonstrated to be a useful tool for addressing the coupled effect of overpressure and conduit erosion on effusion rate. Yet, effusion rates have a much more complex behavior than that proposed by Wadge (1981) (Coppola et al., 2009; Harris et al., 2000; Harris et al., 2011; Ripepe et al., 2015), and additional controlling factors should be considered for properly describing the dynamics of effusive eruptions.

Based on the above arguments, here we study, through numerical simulations, the effects of fluid shear stress and elastic deformation on the evolution of conduit geometry and their consequences on eruptive dynamics. In this model, we consider depth-dependent variations of conduit geometry and magma properties, thus representing a significant step

forward in the analysis of magma ascent dynamics during basaltic effusive eruptions. The main objectives of this work are the description of this model and the illustration of some first insights based on modelling results.

2 Methods

We developed a set of simulations of magma flow along a 10-km-long, vertical conduit with depth-dependent elliptical cross section and input parameters variable with time (e.g., magma reservoir overpressure and water content). Each steady-state simulation is representative of a temporal step and is followed by the update of conduit geometry due to erosion processes and elastic deformation, which are controlled by country rock properties and the profiles of viscosity, pressure and velocity along the conduit. Meanwhile, inlet overpressure depends on the mass of erupted magma, as is water content when zoned magma reservoirs are considered (Colucci et al., 2014; Macedonio et al., 2005). It is important to note that, considering the order of magnitude of erosion rate estimated for basaltic effusive eruptions (i.e., not higher than a few meters per month) (Hulme, 1982; Peterson and Swanson, 1974) and the typical ascent timespans (i.e., some hours), the use of a steady-state conduit model by temporal steps seems to be appropriate. Furthermore, results show that during the timespan required for magma ascent, typical variations of source conditions (inlet pressure and water content) do not exceed 0.2%.

2.1 Conduit model

For numerical modeling, we use a 1D steady-state model currently available on line (https://github.com/demichie/MAMMA) which considers the most important processes experienced by magmas during ascent (Aravena et al., 2018; Aravena et al., 2017; La Spina et al., 2015). The model developments related to this work are associated to the adoption of a depth-dependent dyke-like conduit geometry (already available on line) and the inclusion of appropriate criteria for studying its temporal evolution (section 2.2). Magma is described as a mixture of two phases ($i = 1,2$), characterized by a volume fraction (α_i), density (ρ_i), velocity (u_i) and specific entropy (s_i). Phase 1 includes crystals, dissolved gas and melt, and phase 2 is constituted by exsolved gas bubbles (Fig. S1). Although magma fragmentation is considered in this model, because of the occurrence of outgassing and the presence of a gas exsolution relaxation parameter, the conditions for fragmentation were never reached, and thus we present the portion of the model related to effusive eruptions.

The system of equations includes conservation equations for total mass, momentum, energy, and mass of crystals, dissolved gas and exsolved gas (Eqs. 1-6). It also considers two expressions for controlling magma velocity and the volume fraction of phase 1 (Eqs. 7-8).

$$\frac{\partial}{\partial z}\left(\rho u R_{eq}^2\right) = 0 \tag{1}$$

$$\frac{\partial}{\partial z}\left((\alpha_1\rho_1 u_1^2 + \alpha_1 p_1 + \alpha_2\rho_2 u_2^2 + \alpha_2 p_2)\cdot R_{eq}^2\right) = -\rho g R_{eq}^2 - \frac{8\mu u_1}{f_\epsilon^2} \tag{2}$$

$$\begin{aligned}\frac{\partial}{\partial z}\left(\left(\alpha_1\rho_1 u_1\left(e_1 + \frac{p_1}{\rho_1} + \frac{u_1^2}{2}\right) + \alpha_2\rho_2 u_2\left(e_2 + \frac{p_2}{\rho_2} + \frac{u_2^2}{2}\right) - \rho x_1 x_2 (u_1 - u_2)(s_1 - s_2)T\right)\cdot R_{eq}^2\right) \\ = -\rho g u R_{eq}^2 - \frac{8\mu u_1^2}{f_\epsilon^2}\end{aligned} \tag{3}$$

$$\frac{\partial}{\partial z}\left(\alpha_1\rho_c\alpha_c u_1 R_{eq}^2\right) = -\frac{1}{\tau^{(c)}}\alpha_1\rho_c(\alpha_c - \alpha_c^{eq})R_{eq}^2 \tag{4}$$

$$\frac{\partial}{\partial z}\left(x_d\alpha_1(\rho_1 - \alpha_c\rho_c)u_1 R_{eq}^2\right) = -\frac{1}{\tau^{(d)}}(x_d - x_d^{eq})\alpha_1(\rho_1 - \alpha_c\rho_c)R_{eq}^2 \tag{5}$$

$$\frac{\partial}{\partial z}\left(\alpha_2\rho_2 u_2 R_{eq}^2\right) = \frac{1}{\tau^{(d)}}(x_d - x_d^{eq})\alpha_1(\rho_1 - \alpha_c\rho_c)R_{eq}^2 \tag{6}$$

$$\frac{\partial}{\partial z}\left(\left(\frac{u_1^2}{2} - \frac{u_2^2}{2} + e_1 - e_2 + \frac{p_1}{\rho_1} - \frac{p_2}{\rho_2} - (s_1 - s_2)T\right)\cdot R_{eq}^2\right) = -\frac{8\mu u_1}{\alpha_1\rho_1 f_\epsilon^2} - \frac{\rho}{\rho_1\rho_2}\delta_f(u_1 - u_2)R_{eq}^2 \tag{7}$$

$$\frac{\partial}{\partial z}\left(\rho u \alpha_1 R_{eq}^2\right) = -\frac{1}{\tau^{(p)}}(p_2 - p_1)R_{eq}^2 \tag{8}$$

where z is the vertical coordinate, ρ is mixture density, u is mixture velocity, R_{eq} is equivalent conduit radius (Eq. 9), p_i is pressure of phase i (Eq. 10), g is acceleration of gravity, μ is mixture viscosity, f_ϵ is an eccentricity-dependent factor (Eq. 11) (Costa et al., 2007b), e_i is internal energy of phase i, x_i is mass fraction of phase i, T is mixture temperature, ρ_c is crystal density, α_c is volume fraction of crystals in phase 1, $\tau^{(c)}$ is the crystallization relaxation parameter, α_c^{eq} is the equilibrium value of α_c, x_d is mass fraction of dissolved water in the phase composed of melt and dissolved water, $\tau^{(d)}$ is the exsolution relaxation parameter, x_d^{eq} is the equilibrium value of x_d, δ_f is a drag/permeability factor and $\tau^{(p)}$ is the pressure relaxation parameter.

$$R_{eq} = \sqrt{R_a R_b} \tag{9}$$

$$p_i = \rho_i^2 \frac{\partial e_i}{\partial \rho_i} \tag{10}$$

$$f_\epsilon = \sqrt{\frac{2\sqrt{1-\epsilon^2}}{2-\epsilon^2}} \tag{11}$$

where R_a is semi-major axis, R_b is semi-minor axis and ϵ is conduit cross section eccentricity ($\epsilon = \sqrt{1 - R_b^2/R_a^2}$).

The model requires the adoption of some constitutive equations to describe magma viscosity, water solubility, crystallization, outgassing and equations of state (Text S1).

2.2 Temporal evolution and conduit geometry

We assume that magma reservoir overpressure (p_0) is controlled by (Piombo et al., 2016):

$$\frac{dp_0}{dM_0} = \frac{8\mu_{r0}}{\pi\rho_0 D_0^3} \tag{12}$$

where M_0 is magma reservoir mass, μ_{r0} represents rigidity of reservoir host rocks, ρ_0 is reservoir density and D_0 is reservoir diameter (assumed as spherical). A relation also considering magma compressibility along with rock elasticity has been proposed to compute the evolution of pressure in the reservoir (Anderson and Segall, 2011; Segall et al., 2001). Here, we use Eq. 12 in order to compare our results with the model presented by Piombo et al. (2016), postponing a full integration of magma compressibility and rock elasticity in our magma reservoir formulation to future developments.

As the magma reservoir is continuously evacuated and refilled (Fig. S1), pressure is described by:

$$p_0(t) = p_0(M_e(t), M_i(t)) = p_{0i} - \frac{8\mu_{r0}}{\pi\rho_0 D_0^3}\cdot(M_e(t) - M_i(t)) \tag{13}$$

where $M_e(t)$ and $M_i(t)$ are the evacuated and injected mass of magma in the reservoir, respectively (Eqs. 14-15), p_{0i} is initial overpressure of magma reservoir and t represents the elapsed time.

$$M_e(t) = \int_0^t \rho_0 q_{out}(t) dt \tag{14}$$

$$M_i(t) = \int_0^t \rho_0 q_{in}(t) dt \tag{15}$$

where $q_{out}(t)$ is effusion rate (output of conduit simulations), while $q_{in}(t)$ accounts for the injection of melt in the reservoir.

Eruptions end when the pressure and density conditions of magma reservoir are not capable of counteracting the dissipation forces experienced by magmas during ascent, which can occur either before or after reaching the lithostatic pressure (i.e., overpressure equal to zero). Hence, we imposed the condition that the eruption ends when the effusion rate drops below a critical value (q_c). This is in contrast to the assumption of Piombo et al. (2016) that the eruption ends when overpressure becomes zero. It is worth noting that q_c is typically reached after an abrupt change in the slope of effusion rate versus time (Coppola et al., 2017b).

To include the effect of elastic deformation of the feeding dyke, we assume that (Costa et al., 2007a):

$$R_a(z,t) = R_{a_0}(z,t) + (p_1(z,t) - p_l(z)) \cdot (f_1(z) \cdot R_{a_0}(z,t) + f_2(z) \cdot R_{b_0}(z,t)) \tag{16}$$

$$R_b(z,t) = R_{b_0}(z,t) + (p_1(z,t) - p_l(z)) \cdot (f_2(z) \cdot R_{a_0}(z,t) + f_1(z) \cdot R_{b_0}(z,t)) \tag{17}$$

where $R_{a_0}(z,t)$ and $R_{b_0}(z,t)$ are semi-axes lengths for a non-deformed dyke at a given depth and time, $R_a(z,t)$ and $R_b(z,t)$ are the semi-axes dimensions for a deformed dyke at a given depth and time, $p_1(z,t)$ is pressure of magma at a given depth and time (output of conduit simulations), $p_l(z)$ is the far field pressure at a given depth (assumed as the lithostatic value), $f_1(z) = (2\upsilon(z) - 1)/(2\mu_r(z))$, $f_2(z) = \big(1 - \upsilon(z)\big)/\mu_r(z)$, and $\upsilon(z)$ and $\mu_r(z)$ are the host rock Poisson ratio and rigidity at a given depth, respectively.

Based on Eqs. 16 and 17, and considering known values for $R_a(z,t_{i-1})$, $R_b(z,t_{i-1})$, $p_1(z,t_{i-1})$ and $p_1(z,t_i)$, where t_{i-1} and t_i represent two consecutive time steps, it is possible to update R_a and R_b to the new pressure conditions along the conduit ($R_a^*(z,t_i)$ and $R_b^*(z,t_i)$, hereafter).

The erosion rate due to fluid shear stress at a given depth is estimated by (Macedonio et al., 1994):

$$\dot{E}(z) = k_e \cdot \left(\frac{u(z)}{f_\epsilon(z) \cdot R_{eq}(z)}\right)^2 \cdot \frac{\mu(z) \cdot l_r}{\tau_B} \tag{18}$$

where k_e is a proportionality constant, $u(z)$ is magma velocity at a given depth (output of conduit simulations), $f_\epsilon(z)$ is the eccentricity-dependent factor at a given depth, $R_{eq}(z)$ is the equivalent radius at a given depth, $\mu(z)$ is magma viscosity at a given depth (output of conduit simulations), l_r is the characteristic roughness and τ_B is the country rock yield strength. Following Dragoni and Santini (2007), $\dot{R}_b(z)/\dot{R}_a(z)$ is equal to $R_a(z)/R_b(z)$, and thus we employ appropriate factors to impose the erosion rate for both semi-axes:

$$\dot{R_a}(z) = \dot{E}(z) \cdot \sqrt{R_b(z)/R_a(z)} \tag{19}$$

$$\dot{R_b}(z) = \dot{E}(z) \cdot \sqrt{R_a(z)/R_b(z)} \tag{20}$$

Coupling of elastic deformation and conduit erosion introduces some errors in updating the conduit geometry. One solution to reduce this effect is to employ an iterative method for estimating the pressure profile of the next simulation, but computational times dramatically increase and almost equally accurate solutions can be obtained by adopting appropriate temporal steps (Δt). Hence, we use the following expressions for defining the geometry of

successive simulations:

$$R_a(z, t_{i+1}) = R_a^*(z, t_i) + \Delta t \cdot \dot{R}_a(z) \cdot \left(\frac{R_a^*(z)}{R_a(z)}\right) \quad (21)$$

$$R_b(z, t_{i+1}) = R_b^*(z, t_i) + \Delta t \cdot \dot{R}_b(z) \cdot \left(\frac{R_b^*(z)}{R_b(z)}\right) \quad (22)$$

To avoid abrupt geometric changes between two consecutive simulations, we used a variable temporal step as a function of erosion rate, while elastic deformation-derived geometry modifications were calculated by using time steps that consider the mean values of pressure between successive simulations. We imposed a constant temperature, and fixed or linearly variable dissolved water contents between $w_{p_{0i}}$ and w_0, as a function of the erupted mass ($w_{p_{0i}}$ represents dissolved water content at $t = 0$, and w_0 is dissolved water content when lithostatic pressure is reached). It is worth noting that eroded lithic fragments are not included as source terms in the system of equations, which is justified by the low mass fraction that these fragments represent in the resulting erupted mixture. Tables S2 and S3 present the input parameters used in two sets of simulations, where we test the effect of initial overpressure, erosion coefficient, compositional zoning, conduit rigidity and melt injection on effusion rate. A summary of model variables is present in Table S4.

3 Results

3.1 No injection of melt in magma reservoir

A first set of simulations describes the case of an eruption driven by the progressive emptying of a reservoir with no injection of deeper magma. Figure 1a-b presents the evolution of conduit geometry for the reference Simulation A, by showing its shape at six specific instants. Velocity and viscosity profiles along the conduit (Fig. S2) produce wider conduits and lower eccentricities near the vent (Fig. 1). Indeed, for Simulation A, the mean value of minor semi-axis evolves from 0.2 to ~0.64 m during the simulated event, with minimum and maximum values at eruption end of ~0.58 m and ~1.13 m at the conduit bottom and the vent, respectively (Fig. 2a), while R_b/R_a gradually increases from 0.004 to values between ~0.011 (at the base) and ~0.022 (at the vent). Although magma reservoir volume and erosion coefficient control the erosion rate, final conduit geometries are similar for all the simulations described here (Fig. 1c-f), with a quite abrupt change in the variation rate of equivalent radius at about 2000-3000 m depth, and pronounced modifications of conduit dimensions near the vent. These geometric properties are also observed for shorter conduits (Fig. S3), which tend to reduce dissipation forces and trigger more intense effusive events (Fig. S4). At the eruption onset, simulations show mean increases of semi-minor axis between <0.05 m/month (Simulation H) and ~1.2 m/month (Simulation B), which are consistent with values estimated for natural cases (Hulme, 1982; Peterson and Swanson, 1974). Afterward, because of the overpressure drop and the quadratic dependence of erosion rate and the inverse of equivalent radius, mean erosion rate tends to decrease throughout the eruption, particularly after reaching the maximum effusion rate. Additionally, elastic deformation tends to be more intense nearby and after the peak of effusion rate, producing a significant reduction of conduit dimensions only during final stages of eruptions (Figs. 2b and S5-7). However, given the eruptive parameters considered here, erosion rates are not high enough to produce significant amounts of lithic fragments in the resulting deposits, reaching volume fractions lower than 0.1% for all the simulations.

Effusion rate curves (Fig. 3a-b) present more or less increasing values during the onset of eruptions, and quasi-linearly decreasing trends during the final stages. As expected,

maximum effusion rate is largely controlled by erosion coefficient (Simulations A-B and F-G for comparisons) and magma reservoir dimensions (Simulations A-C and F-H for comparisons). On the other hand, magma reservoirs with a weak compositional zoning produce small differences in the effusion rate (Simulations A-D and F-I for comparisons), while conduit rigidity has a moderate effect on the eruptive dynamics (Simulations A-E and F-J for comparisons), particularly during the final stages of effusive eruptions. Therefore, results show a strong influence of erosion intensity on the evolution of the erupted mass, and thus on magma reservoir overpressure (Fig. 3c-f). Indeed, considering a magma reservoir with a fixed volume of 33.5 km^3 ($D_0 = 4$ km, i.e., excluding Simulations C and H), differences in erosion coefficient, conduit rigidity and compositional zoning can produce variations of up to ~30% and ~55% in the total erupted mass, for initial reservoir overpressures of 50 MPa and 20 MPa, respectively (Fig. 3c-d). The evolution of other eruptive parameters is an additional result of our model. Exit velocity and exsolved gas flow present trends similar to those observed for effusion rate (Fig. S8), but with peaks characterized by a broader shape. Additionally, exit velocities exhibit a more irregular behavior and their peaks occur slightly before the maximum of effusion rate.

Simulations A, B and C represent a sort of equivalent set to cases P5, P6 and P3 of Piombo et al. (2016) (Fig. S9), respectively, showing a similar effect of magma reservoir volume and erosion coefficient on the effusion rate. The ratio between the times required for reaching the maximum effusion rate is highly consistent between the two sets of simulations ($1.0: 0.41: 0.78$ for Simulations A, B and C; and $1.0: 0.41: 0.81$ for Simulations P5, P6 and P3), while larger differences are observed when maximum effusion rate and eruption duration are considered. If we refer to the maximum effusion rates, we obtain ratios of $1.0: 4.33: 0.30$ for Simulations A, B and C and ratios of $1.0: 2.97: 0.43$ for Simulations P5, P6 and P3. The differences are possibly due to the elastic deformation considered in our model, which tends to reduce the effusion rate in a more efficient way for simulations characterized by weak erosion processes (i.e., $C > A > B$). Vice versa, the differences in eruption duration are related to the different criteria adopted to define the eruption end.

3.2 Effect of magma injection in the reservoir

Since volcanic systems are often characterized by open system conditions with emptying and refilling cycles (Andronico et al., 2005; Coppola et al., 2017a; Dzurisin et al., 1984; Landi et al., 2006; Ripepe et al., 2017), we have evaluated the effect of syn-eruptive magma injection in the reservoir. For all the simulations we assumed the same conditions for the magma reservoir, conduit properties and volume of injected material, but considered different input rates and duration of the injection (Table S3 and Fig. 4a-d). Melt injection produces a perturbation in the reservoir overpressure (Fig. 4g) that favors conduit erosion and thus an increase of effusion rate (Fig. 4e). Hence, injection rate can exert a strong control on effusion rate and duration of the eruption (Simulations K, L and N for comparisons), producing differences of up to ~30% for both variables. Conversely, differences in the erupted mass are significantly smaller and do not exceed 8% (Fig. 4f).

4 Discussion and conclusions

Temporal evolution of effusive basaltic eruptions and its relationships with magma source conditions can be effectively analyzed using a steady-state conduit model in an iterative scheme, whenever appropriate criteria for describing fluid shear stress and elastic deformation are considered. The model findings further extend the results of a recently published analytical model (Piombo et al., 2016), and the observed differences can be successfully explained in terms of the different criteria used to define the eruption end and the consideration of elastic

deformation. Still, our model represents a significant step forward in the analysis of the evolution of effusive eruptions, since it allows consideration of (1) depth-varying conduit geometries and their temporal evolution, (2) host rock elastic deformation, (3) compositional zoning of magma reservoirs, (4) depth-dependent conduit mechanical properties, and (5) the injection of deep magma in the reservoir. The model describes several flow variables such as: (1) geometry of the conduit, (2) effusion rate, (3) exit velocity and (4) gas flow, allowing to study a more complete dataset. Moreover, although it is not described here, the conduit model allows description of temporal variations in density, viscosity and crystal content along the conduit, which can be potentially useful for the analysis of specific case studies.

Results indicate that viscosity and velocity profiles along the conduit can produce heterogeneous erosion processes, with higher erosion rates at shallow levels of the conduit. Although magma viscosity and velocity are systematically larger near the vent, there are some counteracting mechanisms able to limit the geometric modifications along the conduit, such as the quadratic dependence between erosion rate and the inverse of the equivalent radius, and the decompression drift experienced by magma reservoirs. The latter tends to reduce magma velocity and thus erosion rate, in addition to a gradually more significant effect of the elastic deformation acting in opposition to fluid shear stress. Since alternative erosion mechanisms are not expected to occur in effusive eruptions (Aravena et al., 2017; Macedonio et al., 1994), we suggest that these geometric properties are representative of actual conduit features during effusive eruptions, whereas conduits with fixed diameters appear to be unrealistic.

The relative balance between conduit widening, elastic deformation and the decreasing trend of magma reservoir overpressure controls the evolution of effusion rate. The onset of eruptions, characterized by low effusion rates and thus slow decompression rates, is mainly influenced by the efficiency of early conduit erosion:

(a) In case of an efficient early erosion mechanism (generated by high values of erosion coefficient, reservoir volume and initial overpressure), the initial stages are characterized by an abrupt increase in effusion rate, which is gradually counterbalanced by the overpressure drop related to magma withdrawal, until the maximum effusion rate is reached. Beyond this point, erosion rate shows an abrupt decrease and, afterward, effusion rate declines as overpressure decreases and elastic relaxation becomes relevant.

(b) In the case of an inefficient early erosion mechanism (i.e., low values of erosion coefficient, reservoir volume and initial overpressure), the initial stages are characterized by quasi-constant effusion rates. Afterward, due to erosion rate decrease and reservoir decompression, a gradual and slow decline of effusion rate is typically observed.

Since eruptions end when dissipation forces are large enough to hinder magma ascent, conduit geometry and thus the efficiency of erosional processes play a major role on the final stages of effusive eruptions, with a strong influence on the total mass that these events are able to evacuate. Moreover, for the range of input parameters considered here, effusion rate exhibits trends similar to those observed for exit velocity and gas flow. Still, it is worth noting that we considered a simplified system, where the temporal variations are limited to conduit geometry, water content and reservoir overpressure, whereas several other kinds of magma source variations have been described for natural cases (Corsaro and Miraglia, 2005), which can alter the curves of effusion rate, exit velocity and gas flow. Moreover, the occurrence of refilling cycles has been proposed as a typical mechanism controlling effusion rate (Coppola et al., 2017a; Ripepe et al., 2017). These processes are expected to depend on complex feedbacks between reservoir overpressure and the deeper feeding system, as well as on the characteristic times required for the displacement of large volumes of magma in the crust. Although our simulations assume a simplified feeding process of the reservoir, results highlight the

importance of the injection rate and the timespan in which it occurs in controlling the eruptive dynamics, even considering a fixed volume of injected material.

All things considered, the systematic analysis of the influence of erosion rate, conduit mechanical parameters and source conditions is able to provide useful information for interpreting measurable characteristics of effusive eruptions, and for inverting these data in order to infer source conditions of specific effusive events. Indeed, several efforts have been made in order to understand, classify and interpret effusion rate trends (Calvari et al., 2003; Harris and Rowland, 2009; Harris et al., 2011). We believe that the model herein presented can substantially contribute both to the study of the typical behavior of these systems and to the analysis of particular effusive eruptions.

Acknowledgments

This paper is a theoretical work and does not contain new data.

References

Anderson, K., and Segall, P., 2011, Physics- based models of ground deformation and extrusion rate at effusively erupting volcanoes: Journal of Geophysical Research: Solid Earth, v. 116, no. B7.

Andronico, D., S. Branca, S. Calvari, M. Burton, T. Caltabiano, R. A. Corsaro, P. Del Carlo, G. Garfì, L. Lodato, and L. Miraglia (2005). A multi-disciplinary study of the 2002–03 Etna eruption: insights into a complex plumbing system. *Bulletin of Volcanology*, 67(4), 314-330.

Aravena, A., M. de' Michieli Vitturi, R. Cioni, and A. Neri (2017). Stability of volcanic conduits during explosive eruptions. *Journal of Volcanology and Geothermal Research*, 339, 52-62.

Aravena, A., R. Cioni, M. de' Michieli Vitturi, and A. Neri (2018). Conduit stability effects on intensity and steadiness of explosive eruptions. *Scientific Reports*, 8, 4125.

Calvari, S., M. Neri, and H. Pinkerton (2003). Effusion rate estimations during the 1999 summit eruption on Mount Etna, and growth of two distinct lava flow fields. *Journal of Volcanology and Geothermal Research*, 119(1), 107-123.

Colucci, S., M. de' Michieli Vitturi, A. Neri, and D. Palladino (2014). An integrated model of magma chamber, conduit and column for the analysis of sustained explosive eruptions. *Earth and Planetary Science Letters*, 404, 98-110.

Coppola, D., D. Piscopo, T. Staudacher, and C. Cigolini (2009). Lava discharge rate and effusive pattern at Piton de la Fournaise from MODIS data. *Journal of Volcanology and Geothermal Research*, 184(1), 174-192.

Coppola, D., M. Ripepe, M. Laiolo, and C. Cigolini (2017a). Modelling satellite-derived magma discharge to explain caldera collapse. *Geology*, 45(6), 523-526.

Coppola, D., A. Di Muro, A. Peltier, N. Villeneuve, V. Ferrazzini, M. Favalli, P. Bachèlery, L. Gurioli, A. Harris, and S. Moune (2017b). Shallow system rejuvenation and magma discharge trends at Piton de la Fournaise volcano (La Réunion Island). *Earth and Planetary Science Letters*, 463, 13-24.

Corsaro, R. A., and L. Miraglia (2005). Dynamics of 2004–2005 Mt. Etna effusive eruption as inferred from petrologic monitoring. *Geophysical Research Letters*, 32(13).

Costa, A. (2005). Viscosity of high crystal content melts: dependence on solid fraction. *Geophysical Research Letters*, 32(22).

Costa, A., O. Melnik, and R. Sparks (2007a). Controls of conduit geometry and wallrock elasticity on lava dome eruptions. *Earth and Planetary Science Letters*, 260(1), 137-151.

Costa, A., O. Melnik, R. Sparks, and B. Voight (2007b). Control of magma flow in dykes on cyclic lava dome extrusion. *Geophysical Research Letters*, 34(2).

Degruyter, W., O. Bachmann, A. Burgisser, and M. Manga (2012). The effects of outgassing on the transition between effusive and explosive silicic eruptions. *Earth and Planetary Science Letters*, 349, 161-170.

Dingwell, D. B., N. Bagdassarov, G. Bussod, and S. L. Webb (1993). Magma rheology. *Mineralogical Association of Canada, Short Course on Experiments at High Pressure and Applications to the Earth's Mantle*, pp. 131–196.

Dragoni, M., and S. Santini (2007). Lava flow in tubes with elliptical cross sections. *Journal of Volcanology and Geothermal Research*, 160(3), 239-248.

Dzurisin, D., R. Y. Koyanagi, and T. T. English (1984). Magma supply and storage at Kilauea Volcano, Hawaii, 1956–1983. *Journal of Volcanology and Geothermal Research*, 21(3-4), 177-206.

Giordano, D., J. K. Russell, and D. B. Dingwell (2008). Viscosity of magmatic liquids: a model. *Earth and Planetary Science Letters*, 271(1), 123-134.

Harris, A., and S. Rowland (2009). Effusion rate controls on lava flow length and the role of heat loss: a review. *Studies in volcanology: the legacy of George Walker*. *Special Publications of IAVCEI*, 2, 33-51.

Harris, A., J. Dehn, and S. Calvari (2007). Lava effusion rate definition and measurement: a review. *Bulletin of Volcanology*, 70(1), 1.

Harris, A., A. Steffke, S. Calvari, and L. Spampinato (2011). Thirty years of satellite- derived lava discharge rates at Etna: Implications for steady volumetric output. *Journal of Geophysical Research: Solid Earth*, 116(B8).

Harris, A., J. Murray, S. Aries, M. Davies, L. Flynn, M. Wooster, R. Wright, and D. Rothery (2000). Effusion rate trends at Etna and Krafla and their implications for eruptive mechanisms. *Journal of Volcanology and Geothermal Research*, 102(3), 237-269.

Hulme, G. (1982). A review of lava flow processes related to the formation of lunar sinuous rilles. *Surveys in Geophysics*, 5(3), 245-279.

La Spina, G., M. Burton and M. de'Michieli Vitturi (2015), Temperature evolution during magma ascent in basaltic effusive eruptions: A numerical application to Stromboli volcano. *Earth and Planetary Science Letters*, 426, 89-100.

Landi, P., L. Francalanci, M. Pompilio, M. Rosi, R. Corsaro, C. Petrone, I. Nardini, and L. Miraglia (2006). The December 2002–July 2003 effusive event at Stromboli volcano, Italy: insights into the shallow plumbing system by petrochemical studies. *Journal of Volcanology and Geothermal Research*, 155(3), 263-284.

Le Métayer, O., J. Massoni, and R. Saurel (2005). Modelling evaporation fronts with reactive Riemann solvers. *Journal of Computational Physics*, 205(2), 567-610.

Llewellin, E., and M. Manga (2005). Bubble suspension rheology and implications for conduit flow. *Journal of Volcanology and Geothermal Research*, 143(1), 205-217.

Macedonio, G., F. Dobran, and A. Neri (1994). Erosion processes in volcanic conduits and application to the AD 79 eruption of Vesuvius. *Earth and Planetary Science Letters*, 121(1), 137-152.

Macedonio, G., A. Neri, J. Martì, and A. Folch (2005). Temporal evolution of flow conditions in sustained magmatic explosive eruptions. *Journal of Volcanology and Geothermal Research*, 143(1), 153-172.

Manga, M., and M. Loewenberg (2001). Viscosity of magmas containing highly deformable bubbles. *Journal of Volcanology and Geothermal Research*, 105(1), 19-24.

Peterson, D. W., and D. A. Swanson (1974). Observed formation of lava tubes. *Studies in Speleology*, 2(6), 209-222.

Piombo, A., A. Tallarico, and M. Dragoni (2016). Role of mechanical erosion in controlling the effusion rate of basaltic eruptions. *Geophysical Research Letters*, 43(17), 8970-8977.

Rhodes, J., and M. Vollinger (2004). Composition of basaltic lavas sampled by phase- 2 of the Hawaii Scientific Drilling Project: Geochemical stratigraphy and magma types. *Geochemistry, Geophysics, Geosystems*, 5(3).

Ripepe, M., D. Delle Donne, R. Genco, G. Maggio, M. Pistolesi, E. Marchetti, G. Lacanna, G. Ulivieri, and P. Poggi (2015). Volcano seismicity and ground deformation unveil the gravity-driven magma discharge dynamics of a volcanic eruption. *Nature Communications*, 6, 6998.

Ripepe, M., M. Pistolesi, D. Coppola, D. Delle Donne, R. Genco, G. Lacanna, M. Laiolo, E. Marchetti, G. Ulivieri, and S. Valade (2017). Forecasting Effusive Dynamics and Decompression Rates by Magmastatic Model at Open-vent Volcanoes. *Scientific Reports*, 7.

Segall, P., Cervelli, P., Owen, S., Lisowski, M., and Miklius, A., 2001, Constraints on dike propagation from continuous GPS measurements: Journal of Geophysical Research: Solid Earth, v. 106, no. B9, p. 19301-19317.

Smith, P. M., and P. D. Asimow (2005). Adiabat_1ph: A new public front- end to the MELTS, pMELTS, and pHMELTS models. *Geochemistry, Geophysics, Geosystems*, 6(2).

Wadge, G. (1981). The variation of magma discharge during basaltic eruptions. *Journal of Volcanology and Geothermal Research*, 11(2-4), 139-168.

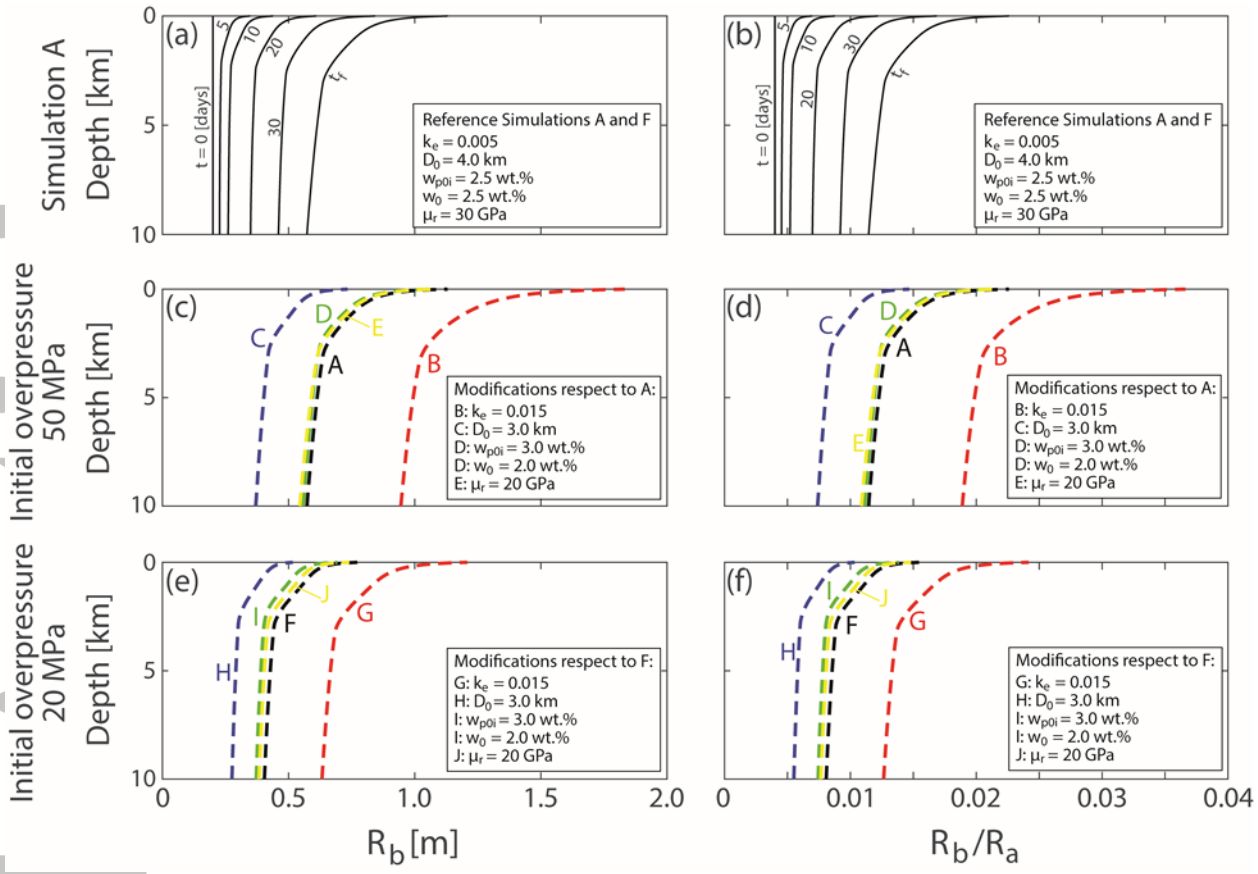

Figure 1. Evolution of conduit geometry for Simulations A-J. (a) Semi-minor axis at different times (Simulation A). (b) Ratio between semi-minor and semi-major axes at different times (Simulation A). (c) Semi-minor axis at eruptions' end (Simulations A-E). (d) Ratio between semi-minor and semi-major axes at eruptions' end (Simulations A-E). (e) Semi-minor axis at eruptions' end (Simulations F-J). (f) Ratio between semi-minor and semi-major axes at eruptions' end (Simulations F-J).

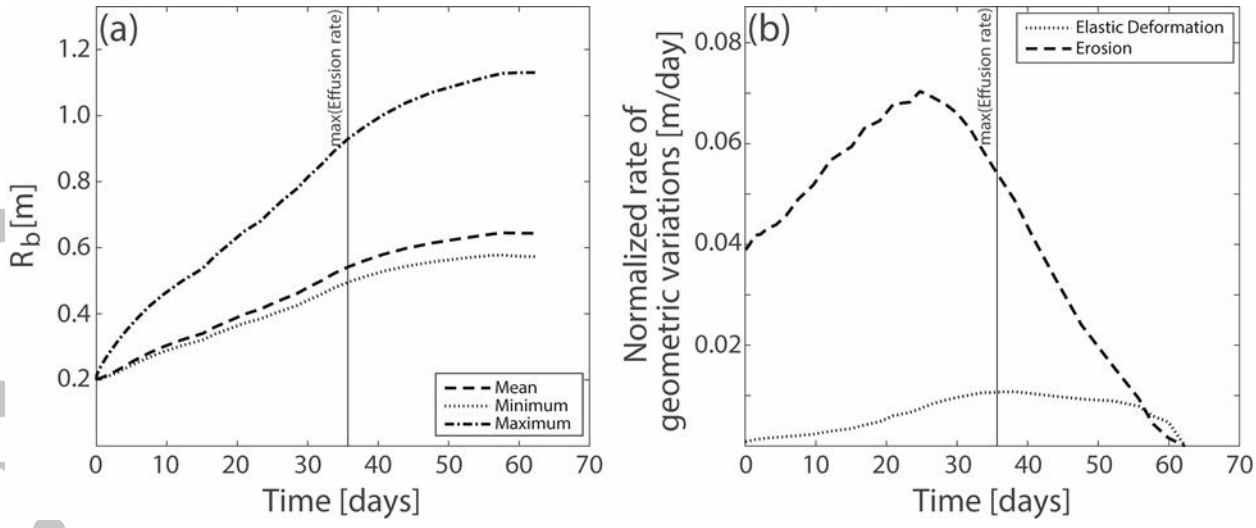

Figure 2. (a) Semi-minor axis versus elapsed time (Simulation A). (b) Normalized rate of geometric variation by erosion and elastic deformation versus elapsed time, considering the average values along the conduit (Simulation A). For calculating these functions, for each step, we split the rate of geometric variation ($\Delta R_{eq}/\Delta t$) in two contributions: fluid shear stress and elastic deformation. Fluid shear stress tends to increase conduit dimensions, in opposition to elastic deformation (negative contribution, the absolute value is plotted).

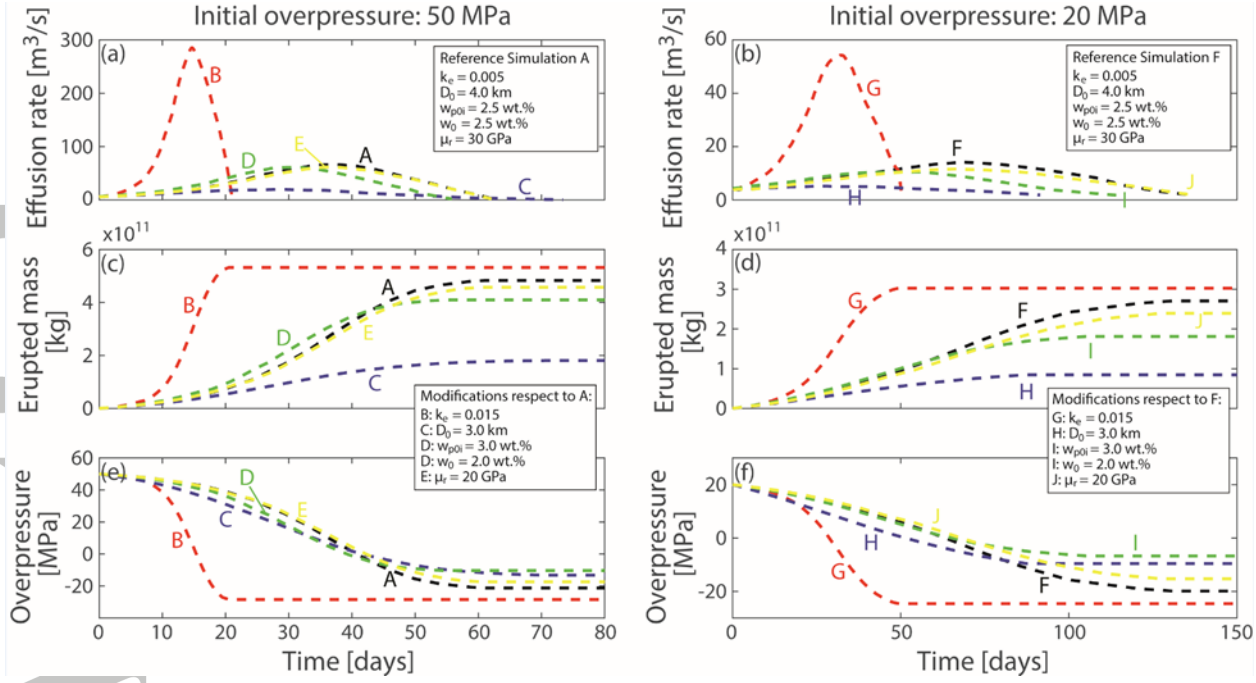

Figure 3. Temporal evolution of effusion rate, erupted mass and reservoir overpressure. **Left hand-side:** Simulations A-E. **Right hand-side:** Simulations F-J.

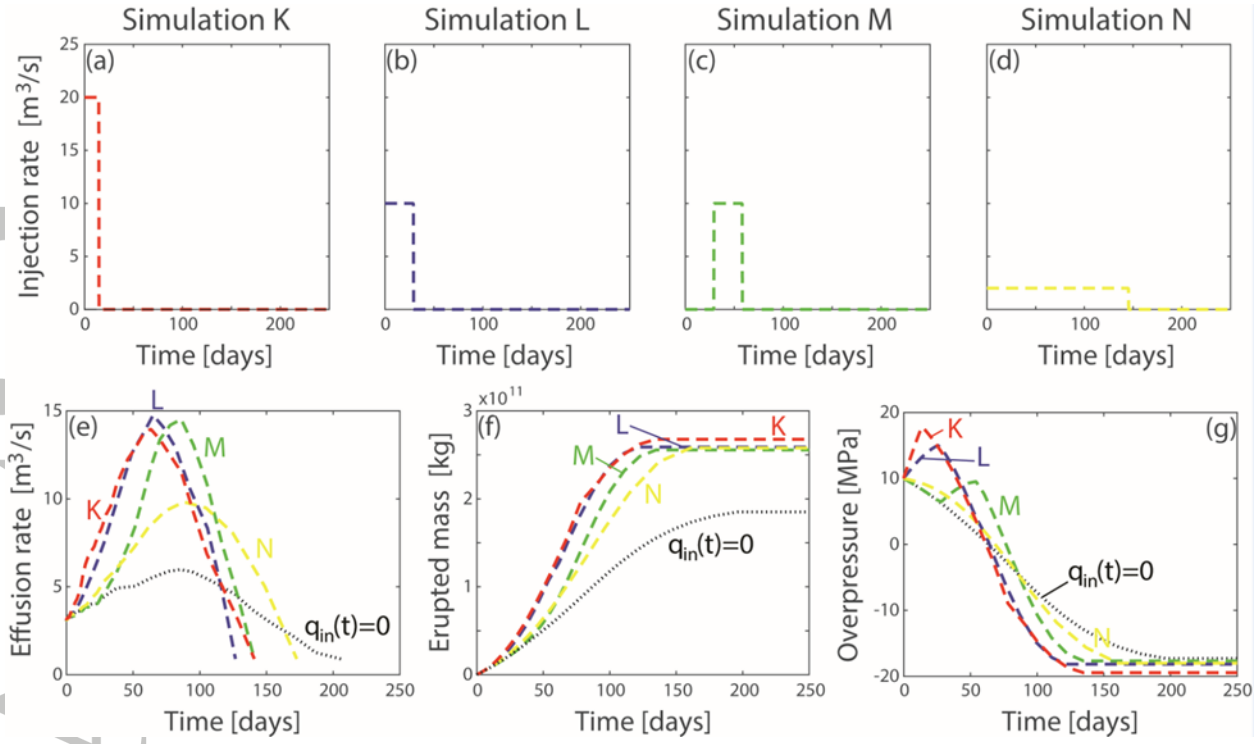

Figure 4. Temporal evolution of key eruptive parameters for Simulations K-N. Results associated to the equivalent simulation with no melt injection are also included. (a-d) Melt injection in the reservoir. (e) Effusion rate. (f) Erupted mass. (g) Reservoir overpressure.